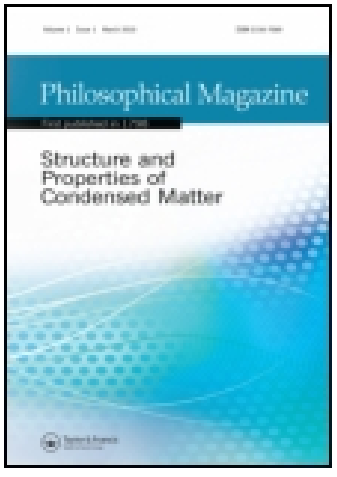

Philosophical Magazine
Publication details, including instructions for authors and subscription information:
http://www.tandfonline.com/loi/tphm20

Σ3 CSL boundary distributions in an austenitic stainless steel subjected to multidirectional forging followed by annealing

Marina Tikhonova[a], Yuliya Kuzminova[a], Xiaoying Fang[b], Weiguo Wang[c], Rustam Kaibyshev[a] & Andrey Belyakov[a]

[a] Laboratory of Mechanical Properties of Nanostructured Materials and Superalloys, Belgorod State University, Pobeda 85, Belgorod 308015, Russia

[b] School of Mechanical Engineering, Shandong University of Technology, Zibo, China

[c] College of Materials Science and Engineering, Fujian University of Technology, Fujian, China

Published online: 20 Nov 2014.

To cite this article: Marina Tikhonova, Yuliya Kuzminova, Xiaoying Fang, Weiguo Wang, Rustam Kaibyshev & Andrey Belyakov (2014) Σ3 CSL boundary distributions in an austenitic stainless steel subjected to multidirectional forging followed by annealing, Philosophical Magazine, 94:36, 4181-4196, DOI: 10.1080/14786435.2014.982743

To link to this article: http://dx.doi.org/10.1080/14786435.2014.982743

Philosophical Magazine, 2014
Vol. 94, No. 36, 4181–4196, http://dx.doi.org/10.1080/14786435.2014.982743

Σ3 CSL boundary distributions in an austenitic stainless steel subjected to multidirectional forging followed by annealing

Marina Tikhonova[a], Yuliya Kuzminova[a], Xiaoying Fang[b], Weiguo Wang[c], Rustam Kaibyshev[a] and Andrey Belyakov[a]*

[a]*Laboratory of Mechanical Properties of Nanostructured Materials and Superalloys, Belgorod State University, Pobeda 85, Belgorod 308015, Russia;* [b]*School of Mechanical Engineering, Shandong University of Technology, Zibo, China;* [c]*College of Materials Science and Engineering, Fujian University of Technology, Fujian, China*

(*Received 14 June 2014; accepted 26 October 2014*)

The effect of processing and annealing temperatures on the grain boundary characters in the ultrafine-grained structure of a 304-type austenitic stainless steel was studied. An S304H steel was subjected to multidirectional forging (MDF) at 500–800°C to total strains of ~4, followed by annealing at 800–1,000°C for 30 min. The MDF resulted in the formation of ultrafine-grained microstructures with mean grain sizes of 0.28–0.85 μm depending on the processing temperature. The annealing behaviour of the ultrafine-grained steel was characterized by the development of continuous post-dynamic recrystallization including a rapid recovery followed by a gradual grain growth. The post-dynamically recrystallized grain size depended on both the deformation temperature and the annealing temperature. The recrystallization kinetics was reduced with an increase in the temperature of the preceding deformation. The grain growth during post-dynamic recrystallization was accompanied by an increase in the fraction of $\Sigma 3^n$ CSL boundaries, which was defined by a relative change in the grain size, i.e. a ratio of the annealed grain size to that evolved by preceding warm working (D/D_0). The fraction of $\Sigma 3^n$ CSL boundaries sharply rose to approximately 0.5 in the range of D/D_0 from 1 to 5, which can be considered as early stage of continuous post-dynamic recrystallization. Then, the rate of increase in the fraction of $\Sigma 3^n$ CSL boundaries slowed down significantly in the range of $D/D_0 > 5$. A fivefold increase in the grain size by annealing is a necessary condition to obtain approximately 50% $\Sigma 3^n$ CSL boundaries in the recrystallized microstructure.

Keywords: EBSD; austenitic stainless steels; ultrafine grains; recrystallization; grain growth; annealing twins; grain boundaries

1. Introduction

The grain boundary character distributions in structural materials are important for their properties. The development of a beneficial distribution of grain boundaries on their character is one aim of grain boundary engineering [1–5]. In particular, the goal of grain boundary engineering is to control the fraction of special boundaries that are characterized by a low reciprocal density of coinciding sites, Σ, of the coincident site lattice

*Corresponding author. Email: belyakov@bsu.edu.ru

(CSL). Coherent Σ3 CSL boundaries have lower energies than ordinary grain boundaries and therefore possess some beneficial properties [6–8].

In face-centred cubic metals and alloys with low stacking fault energy (SFE), the evolution of special boundaries is associated with the development of annealing twins with coherent Σ3 CSL boundaries [5,9–11]. The development of multiple twinning that results in a spatial net of $\Sigma 3^n$ CSL boundaries is a key factor in the design of grain boundary-engineered microstructures in such materials. Generally, the formation of annealing twins is associated with thermally activated grain boundary migration, e.g. recrystallization, which frequently takes place during annealing at elevated temperatures. It has been shown that fractions of $\Sigma 3^n$ CSL boundaries well above 0.5 in austenitic stainless steels can be easily obtained by high-temperature annealing after cold straining to low values of 3–5% [6,7]. The annealed microstructures are characterized by a large fraction of $\Sigma 3^n$ grain clusters and an effective interruption of the connectivity of the random high-angle boundary network by twin-related boundaries [12]. The structural mechanism responsible for the development of such microstructures is primary recrystallization, which involves long-range grain boundary migration and therefore leads to the development of relatively coarse-grained microstructures concurrently with the formation of numerous $\Sigma 3^n$ CSL boundaries.

A disadvantage of coarse-grained steels and alloys is their low yield strength, which significantly limits their application as structural materials. The mechanical properties of structural metallic materials can be enhanced by grain refinement. Ultrafine-grained materials with an average grain size below 1 μm have been suggested to possess a unique combination of high strength and sufficient ductility that has aroused great interest in their production [13–16]. One of the most promising methods for obtaining ultrafine-grained steels and alloys is large strain plastic working [17–20]. Ultrafine-grained structures can be achieved in various metals and alloys through continuous dynamic recrystallization under warm-working conditions which results in the progressive development of ultrafine grains rather than deformation subgrains [21–25]. In austenitic stainless steels, the continuously recrystallized microstructures are characterized by a very low fraction of Σ3 CSL boundaries because the boundaries in ultrafine-grained microstructures develop without any long-range boundary migration [26,27]. Generally, the fraction of special boundaries in warm-worked stainless steels can be increased by subsequent static recrystallization. The annealing behaviour of submicrocrystalline stainless steel processed by large strain deformation has been interpreted as continuous static recrystallization, which could be utilized for the development of fully recrystallized ultrafine-grained microstructures [28,29]. However, the development of grain boundary assemblies in ultrafine-grained austenitic stainless steels under conditions of continuous static recrystallization has not been detailed.

The aim of the present work was to study the effect of processing conditions on the grain boundary distribution in ultrafine-grained austenitic stainless steel subjected to large strain warm working followed by annealing. This study focused particularly on the evaluation of the critical conditions required for the development of a large fraction of $\Sigma 3^n$ CSL boundaries in ultrafine-grained stainless steel.

2. Experimental

An S304H austenitic stainless steel, 0.10%C–18.2%Cr–7.85%Ni–2.24%Cu–0.50%Nb–0.008%B–0.12%N–0.95%Mn–0.10%Si and the balance Fe (in weight%) with an

average grain size of ~10 μm was used as the starting material. Rectangular samples with initial dimensions of 10 mm × 12.2 mm × 15 mm were machined for multidirectional forging (MDF), which was carried out by performing isothermal multipass compression tests with a change in the compression direction of 90° in order of the three orthogonal axes from pass to pass [15,21,27]. The samples were compressed at temperatures of 500, 600, 700, and 800°C at a strain rate of 10^{-3} s^{-1} to a strain of 0.4 in each pass. The compressed samples were quenched in water, machined to rectangular shapes and then reheated to the test temperature. Lastly, the samples subjected to MDF to a total strain of four were annealed for 30 min at temperatures of 800, 900 and 1,000°C. Structural investigations were carried out on the sample sections parallel to the compression axis of the final compression pass using an FEI Quanta 600F scanning electron microscope equipped with an electron backscatter diffraction (EBSD) analyzer incorporating an orientation imaging microscopy (OIM) system. The EBSD map size was 20 μm × 20 μm for the MDF samples and the samples annealed at 800°C, 50 μm × 50 μm for the samples annealed at 900°C and 60 μm × 60 μm for the samples annealed at 1,000°C. The step size for the EBSD scans was 50 nm for the samples subjected to MDF and the samples annealed at 800°C and 300 nm for the samples annealed at a range 900–1,000°C. The total number of grains analysed per EBSD map was ~1,000–3,000 in the as-deformed state and 300–600 in the annealed samples. The OIM images were subjected to clean-up procedures, setting a minimal confidence index of 0.1. The average fraction of points modified by clean-up procedure was ~0.12 in the as-deformed samples and ~0.03 in the annealed samples. The grain boundary distributions and the fractions of $\Sigma 3^n$ CSL boundaries were evaluated by OIM software (EDAX TSL, ver. 5). The high-angle boundary spacing and the grain size were measured using linear intercept method on the OIM images for the distance between the high-angle boundaries (HABs), i.e. those with misorientations of $\theta \geq 15°$. Note that only ordinary grain boundaries with $\theta \geq 15°$ were taken into account for the grain size measurements, i.e. the $\Sigma 3^n$ CSL boundaries were omitted.

3. Results

3.1. *Deformation microstructures*

Representative images of grain boundary distributions evolved by MDF to total strains of four at different temperatures are shown in Figure 1. The 10 forging passes resulted in the formation of nearly full ultrafine-grained microstructures. The mean grain size in the highly strained steel samples increased from 0.25 to 0.72 μm with increasing temperature from 500 to 800°C. The ultrafine grain evolution was not accompanied by the development of any strong textures; the ultrafine-grained microstructures exhibited nearly random crystallographic orientations (Figure 1). Figure 2 shows the distributions of kernel average misorientations, which can be used for rough estimation of internal stresses in the ultrafine-grained microstructures evolved by MDF. In general, the kernel average misorientations were homogeneously distributed in the ultrafine-grained samples, and the values of internal distortions increased as the MDF temperature decreased. Almost all grains in the sample processed by MDF at 800°C were characterized by small kernel average misorientations below 1° the fraction of larger misorientations did not exceed 0.1. The fraction of kernel average misorientations above 1° remarkably increased in the samples subjected to MDF at lower temperatures. The fraction of

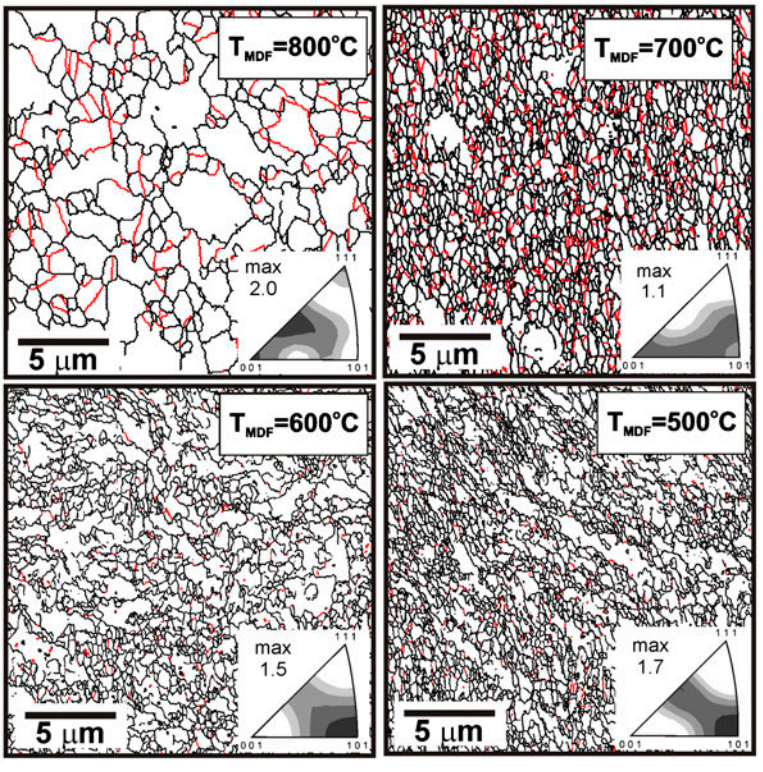

Figure 1. (colour online) Typical microstructures evolved in the S304H austenitic stainless steel subjected to MDF at $T_{MDF} = 800°C$, 700°C, 600°C and 500°C. The red and black lines correspond to the CSL $\Sigma 3^n$ boundaries and ordinary grain boundaries, respectively. The inverse pole figures are shown for the final pass forging axis.

kernel average misorientations in the range of 1–2° comprised ~0.2 after MDF at 700°C and ~0.25 after MDF at 500–600°C. Therefore, the finer grains evolved by MDF at lower temperature experienced larger internal distortions.

Depending on the deformation temperature, the developed microstructures were characterized by somewhat different distributions of grain boundary misorientations (Figure 3). At all temperatures, there were a number of low-angle subboundaries which is also an indicative of continuous dynamic recrystallization as the structural mechanism of ultrafine grain evolution during MDF [27,30–32]. The height of the peak corresponding to low-angle subboundaries decreased with increasing temperature. The ordinary high-angle grain boundaries (i.e. those with misorientations of $\theta \geq 15°$ excluding $\Sigma 3$ CSL boundaries) that developed during MDF at 500–600°C were characterized by flat-type misorientation distributions with nearly the same fractions of various misorientations as indicated by solid lines in Figure 3. On the other hand, the grain boundary misorientation distributions evolved at 700–800°C exhibited rather sharp peaks at 60° misorientations, and the height of this maximum increased with the deformation temperature. The peak of 60° misorientations mainly originated from $\Sigma 3$ CSL boundaries of annealing twins. Increasing the deformation temperature promoted the discontinuous

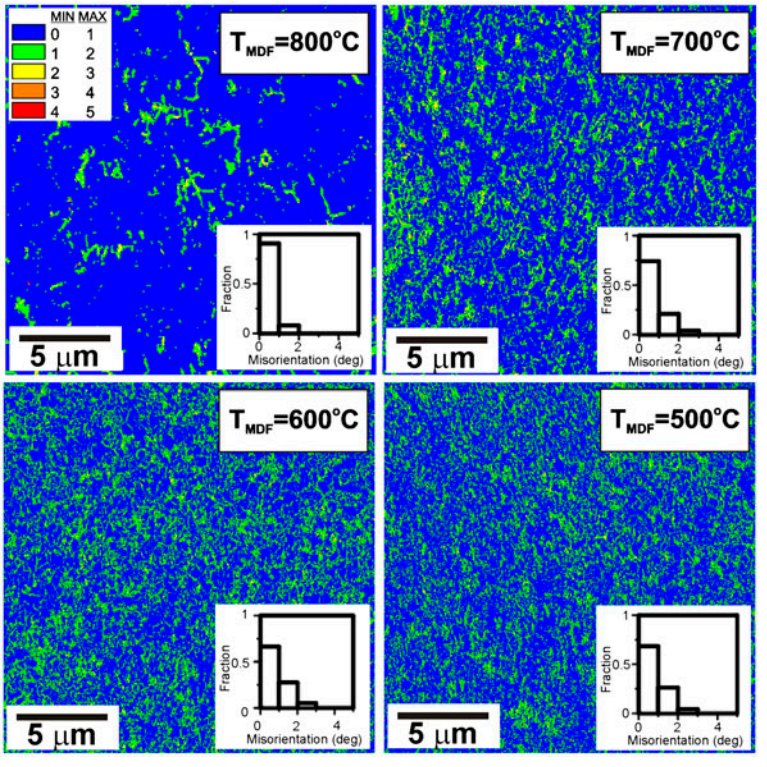

Figure 2. (colour online) The kernel average misorientation distributions evolved in the S304H austenitic stainless steel subjected to MDF at T_{MDF} = 800°C, 700°C, 600°C and 500°C.

recrystallization mechanism, which is associated with a bulging and long range migration of grain boundaries [27,33], leading to an increase in the number of annealing twins. In contrast to MDF at 500–600°C, the misorientation distributions of ordinary grain boundaries evolved at 700–800°C are close to random (Mackenzie [34]) distribution, which is also indicated in Figure 3 by dashed lines.

3.2. *Annealed microstructures*

Typical annealed grain boundary distributions that developed in the steel samples subjected to MDF are shown in Figure 4. Annealing generally results in a slight increase in grain size indicating the development of static or post-dynamic recrystallization. The results clearly show that annealing at 800°C did not lead to significant grain coarsening. The grain size remained on the micron scale in all samples irrespective of the temperature of the preceding MDF. Increasing the annealing temperature promoted the grain coarsening. Nevertheless, the steel samples can be classified as being fine grained even after annealing at such a high temperature as 1,000°C. The annealed microstructures do not exhibit any strong texture. Therefore, any selective grain growth scarcely occurred during annealing. It should also be noted in Figure 4 that the steel samples subjected to

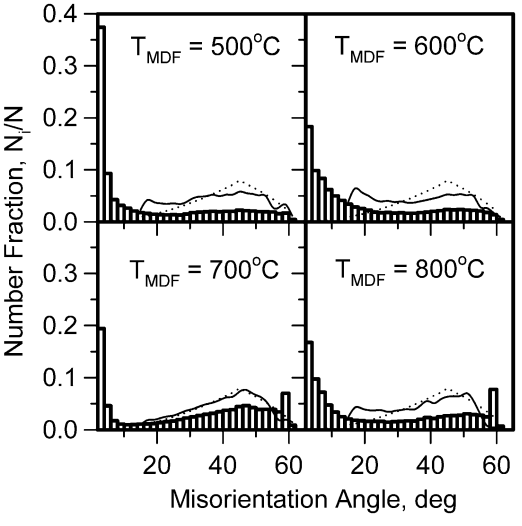

Figure 3. The distributions of the grain boundary misorientations developed in the S304H austenitic stainless steel subjected to MDF at T_{MDF} = 800°C, 700°C, 600°C and 500°C. The solid lines indicate the misorientation distribution of ordinary grain boundaries with misorientations $\theta \geq 15°$ excluding Σ3 CSL boundaries; and the random misorientation distribution is indicated by the dashed lines.

MDF at 800°C are characterized by finer annealed grains than those previously processed at 500°C. Therefore, increasing the temperature of preceding MDF slowed down the kinetics of post-dynamic recrystallization. The grain coarsening during the post-dynamic recrystallization was accompanied by the development of numerous $\Sigma 3^n$ CSL boundaries. It is clearly seen in Figure 4 that the density of the special $\Sigma 3^n$ CSL boundaries decreases with increase in the annealed grain size, although the number of the special boundaries per a grain slightly increases.

The development of post-dynamic recrystallization in the MDF samples was accompanied by a specific change in the grain boundary misorientation distributions (Figure 5). Qualitatively, the changes in the misorientation distributions after annealing are associated with a decrease in the peaks at small angles below 10° and the appearance/rise of sharp peaks for 60° misorientations. However, quantitative changes in the misorientation distributions depend on both the temperature of the preceding MDF and the annealing temperature. After annealing at 800°C, the small-angle peak disappeared completely in the sample forged at 500°C, whereas the fraction of 60° misorientations rose to 0.4 accompanied by the appearance of a small peak at 39°. On the other hand, the samples forged at higher temperatures exhibited remarkably high fractions of low-angle boundaries, and the fraction of 60° misorientations was approximately 0.1. Irrespective of the MDF temperature, the peaks corresponding to low-angle boundaries were removed by increasing the annealing temperature to 900–1,000°C. Correspondingly, all samples annealed at elevated temperatures were characterized by sharp peaks for 60° misorientations. It is interesting to note that increase in the fraction of 60° misorientations during annealing at a range of 800–900°C was accompanied by the development of small

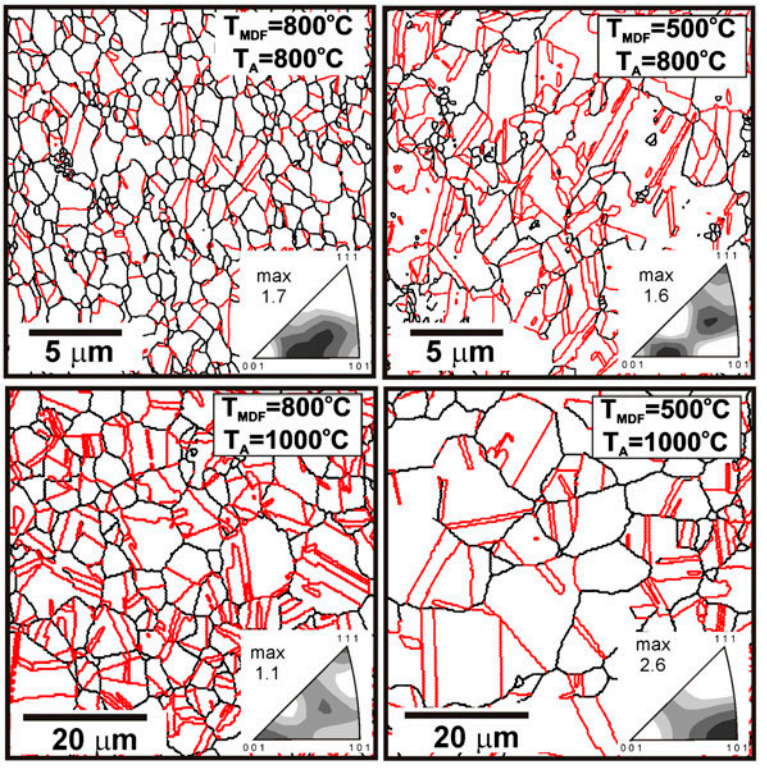

Figure 4. (colour online) Typical microstructures evolved in the S304H austenitic stainless steel subjected to MDF at T_{MDF} = 800°C and 500°C and annealing at T_A = 800°C and 1,000°C. The red and black lines correspond to the $\Sigma 3^n$ CSL boundaries and ordinary grain boundaries, respectively. The inverse pole figures are shown for the last pass forging axis.

peaks at 39°, whereas the latter ones were not observed after annealing at higher temperature of 1,000°C. In all cases, the ordinary high-angle grain boundaries tended to random misorientation distribution (cf. the solid and dashed lines in Figure 5).

Figure 6 presents the quantitative data obtained for the change in grain size, HAB spacing and development of $\Sigma 3^n$ CSL boundaries. The mean grain size in the annealed samples generally increased with increasing annealing temperature. Uniform microstructures with a grain size of 0.7–1.7 μm were obtained after annealing at 800°C. The largest grain size of 1.7 μm is observed in the sample subjected to MDF at the lowest temperature of 500°C, whereas annealed grain sizes of 0.7–1.0 μm evolved in the samples after MDF at 600–800°C. Annealing at 900°C increased the mean grain size to 2–3.3 μm. An interesting effect of the temperature of the preceding MDF on the final grain size was observed after annealing at 1,000°C. The smallest grain size of 5 μm was obtained in the sample forged at the highest temperature of 800°C, while the mean grain sizes in the samples forged at 500–700°C increased to approximately 8 μm. The change in the HAB spacing after annealing of ultrafine-grained samples exhibited the similar temperature dependency as for the mean grain size, although the HAB spacing corresponds to about

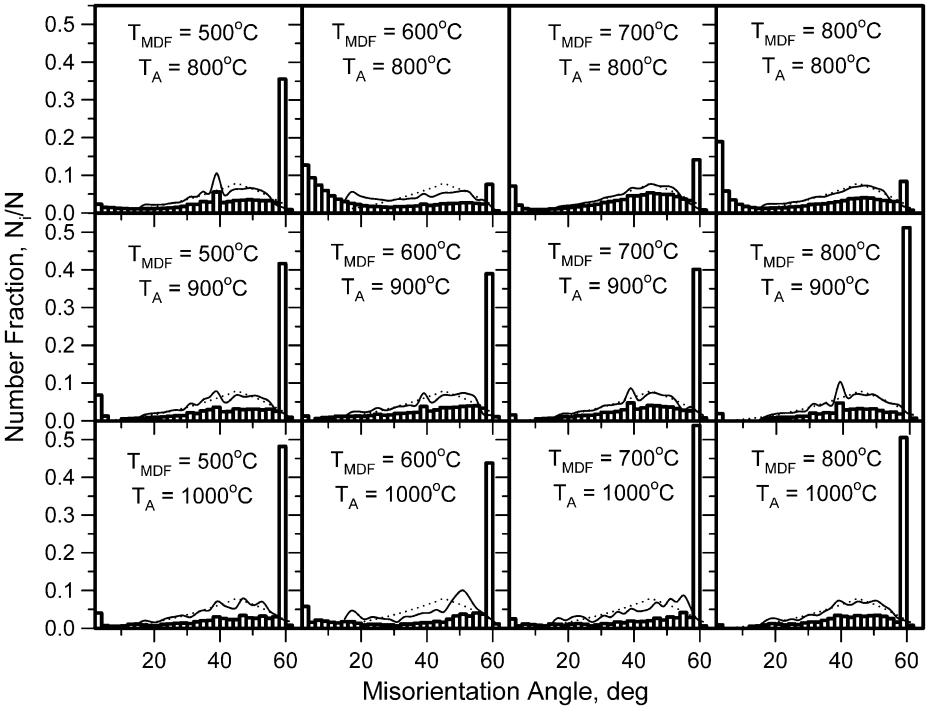

Figure 5. The distributions of the grain boundary misorientations developed in the S304H austenitic stainless steel subjected to MDF and annealing at 800°C, 900°C and 1,000°C. The solid lines indicate the misorientation distribution of ordinary grain boundaries with misorientations $\theta \geq 15°$ excluding Σ3 CSL boundaries and the random misorientation distribution is indicated by the dashed lines.

half of the grain size. It should only be noted that all samples annealed at 800°C were characterized by almost the same HAB spacing of 0.5–0.8 μm.

After annealing at 800°C, the fraction of $\Sigma 3^n$ CSL boundaries increased to 0.45 in the sample subjected to MDF at 500°C. In contrast, remarkably smaller values of $\Sigma 3^n$ CSL boundary fraction of about 0.2 were obtained in the samples forged at higher temperatures, i.e. 600–800°C. The fraction of $\Sigma 3^n$ CSL boundaries increased with annealing temperature and tended to saturate at approximately 0.6 in all samples irrespective of the temperature of the preceding MDF. Thus, all samples annealed at temperatures of 900–1,000°C were characterized by nearly the same fractions of $\Sigma 3^n$ CSL boundaries.

The effects of the forging and annealing temperatures on the microstructure evolution can be more clearly revealed by the changes in the grain size (D) and $\Sigma 3^n$ CSL boundary fraction (F_{CSL}) in reference to their initial values, i.e. those, which were obtained by MDF, D/D_0 and F_{CSL}/F_{CSL0}, respectively (Figure 7). Annealing at 800°C was characterized by slow recrystallization kinetics in the samples processed by MDF at 600–800°C. Relatively fast grain growth was observed for the sample subjected to MDF at 500°C, in which the grain size increased sevenfold after annealing. Other samples demonstrated insignificant grain growth at 800°C. Increasing the annealing temperature to 900–1,000°C led to remarkable grain coarsening in all samples. It is interesting

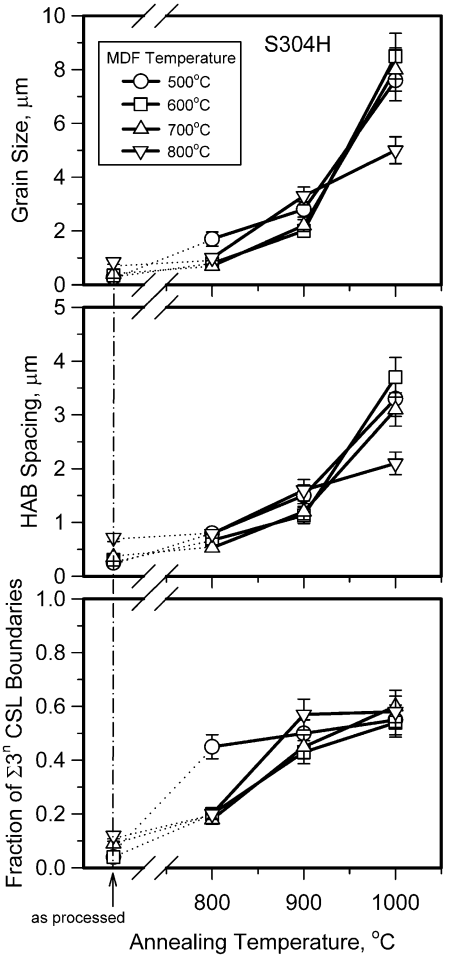

Figure 6. Effects of the annealing temperature on the grain size, the HAB spacing and the fraction of $\Sigma 3^n$ CSL boundaries in the S304H austenitic stainless steel subjected to MDF and annealing.

that samples subjected to MDF at 500–700°C demonstrated nearly the same and rather fast grain coarsening, whereas the sample previously processed at 800°C exhibited quite sluggish recrystallization kinetics even at 1,000°C. Therefore, the kinetics of post-dynamic recrystallization that occurred in ultrafine-grained structures, which were developed by large strain deformation, slowed down with increase in the temperature of the preceding deformation. This effect of the deformation temperature on the following recrystallization can be associated with the different internal stresses in the samples subjected to MDF at different temperatures (Figure 2).

The relative changes in the fraction of $\Sigma 3^n$ CSL boundaries (F_{CSL}/F_{CSL0} in Figure 7) were clearly correlated with the relative changes in the grain sizes. Namely, significant increase in the fraction of $\Sigma 3^n$ CSL boundaries after annealing was observed in the samples subjected to MDF at 500°C, whereas samples previously processed by MDF at

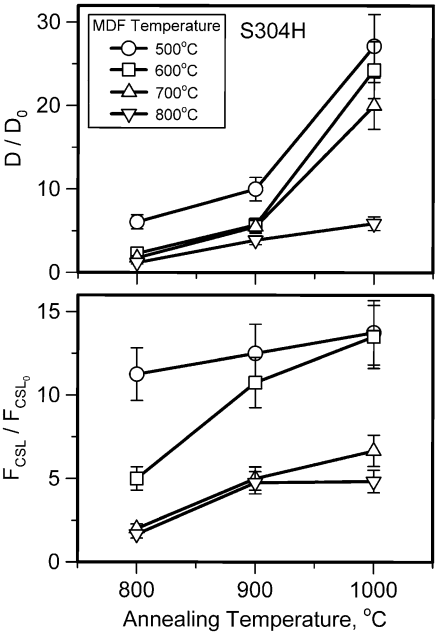

Figure 7. The changes in grain size (D/D_0) and fraction of CSL $\Sigma 3^n$ boundaries (F_{CSL}/F_{CSL0}) in the S304H austenitic stainless steel subjected to MDF and annealing at different temperatures.

800°C were characterized by the smallest increment in the $\Sigma 3^n$ CSL boundary fractions irrespective of the annealing temperature. Correspondingly, the samples, which were forged at 600–700°C, exhibited intermediate behaviours. The limited grain growth at 800°C in these samples was accompanied by insignificant change in fraction of special boundaries, while the acceleration of grain coarsening with increase in the annealing temperature to 900–1,000°C led to remarkable increase in the F_{CSL}/F_{CSL0} ratios, especially for the sample subjected to MDF at relatively low temperature, i.e. 600°C (Figure 7).

4. Discussion

The recrystallization phenomenon that typically occurs in work-hardened metals and alloys upon annealing is considered to be primary static recrystallization, which involves the formation of fine dislocation-free grains (nuclei) in certain parts of the specimen and the subsequent growth of these recrystallization nuclei consuming work-hardened surroundings [35,36]. In the case of ultrafine-grained materials produced by severe plastic deformation, all of the ultrafine grains may serve as recrystallization nuclei during subsequent annealing [28,29]. Therefore, the development of static recrystallization in severely strained materials is associated with a rapid recovery followed by gradual coarsening of the recovered ultrafine grains, and this phenomenon is frequently considered to be continuous static recrystallization or continuous post-dynamic recrystallization because the original ultrafine-grained microstructure is developed by means of continuous dynamic recrystallization during large strain plastic deformation [37].

The appearance of $\Sigma 3^n$ CSL boundaries in stainless steel during annealing is closely related with grain boundary migration, which is accompanied by the formation of annealing twins [10,12]. The small peaks at 39° on the boundary misorientation distributions after annealing at 800–900°C corresponds to increased fraction of Σ9 CSL boundaries, which indicate the multiple annealing twinning at an early stage of continuous post-dynamic recrystallization. In contrast, only the peaks of Σ3 CSL boundaries sharply stand out in the samples annealed at 1,000°C, which are characterized by relatively large grains. This suggests that the development of annealing twins slows down as the recrystallized grains coarsen. Similar results were obtained in other studies on the annealing twin development [38–40]. A rapid increase in twin density was observed during the recrystallization development [40], whereas subsequent grain growth was accompanied by an apparent decrease in the twin density [39]. Nevertheless, the density of ordinary grain boundaries decreases faster than the twin density during recrystallization/grain growth (Figure 6). The fraction of $\Sigma 3^n$ CSL boundaries, therefore, should increase with the size of recrystallized grains.

The obtained results suggest that the increase in the fraction of special boundaries during continuous post-dynamic recrystallization correlates with the change in the grain size during annealing (Figure 7). Let us consider the relationship between the grain growth and the fraction of annealing twins. It is generally agreed that annealing twins form by growth accidents of a migrating grain boundary [41]. Therefore, the probability of twin appearance depends on the velocity of boundary migration [42,43] which in turn is directly proportional to the driving pressure [36,42]. Commonly, the driving pressure (P) for grain growth is related to the boundary surface area and, therefore, is inversely proportional to the grain size (D) [36,42]:

$$P \sim \frac{1}{D} \tag{1}$$

In fact, the samples subjected to MDF at lower temperature, i.e. those having finer grain size, exhibit faster grain growth kinetics upon subsequent annealing (Figure 7). The number of twin boundaries within one growing grain can be estimated by a summation of the initial number of twin boundaries (N_{CSL0}), i.e. twins within a grain before growth occurs, and the number of twin boundaries (N_{CSL}) that evolved during grain growth (Figure 8). The latter can be evaluated by integrating Equation (1) over grain sizes from D_0 to D,

$$N_{CSL} = K \ln \frac{D}{D_0} \tag{2}$$

where K varies from zero upward depending on SFE, i.e. higher K values correspond to lower SFE. In metals and alloys with high SFE like aluminium, the K values are close to zero that means that there are no annealing twins. Taking the twin density as $p = N_{CSL}/D$, Pande et al. [42] obtained $p = (K/D)\ \ln\ (D/D_0)$, which is consistent with experimental data for the change in the twin density during grain growth [39,42,44]. The number fraction of $\Sigma 3^n$ CSL boundaries (F_{CSL}) in the annealed microstructure can be estimated by a ratio of the number of $\Sigma 3^n$ CSL boundaries in a grain to the total number of boundaries per grain:

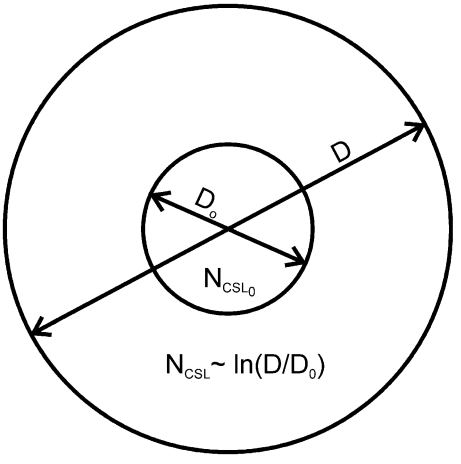

Figure 8. The number of $\Sigma 3^n$ CSL boundaries in a growing grain.

$$F_{\mathrm{CSL}} = \frac{N_{\mathrm{CSL}_0} + K \ln \frac{D}{D_0}}{N_{\mathrm{CSL}_0} + K \ln \frac{D}{D_0} + 1} \tag{3}$$

Taking N_{CSL0} as $(F_{\mathrm{CSL0}}{}^{-1} - 1)^{-1}$, where F_{CSL0} is the number fraction of $\Sigma 3^n$ CSL boundaries in the initial microstructure (i.e. before the grain growth), the change in the fraction of $\Sigma 3^n$ CSL boundaries during annealing reads:

$$\frac{F_{\mathrm{CSL}}}{F_{\mathrm{CSL}_0}} = \frac{K(F_{\mathrm{CSL}_0}^{-1} - 1) \ln \frac{D}{D_0} + 1}{K(1 - F_{\mathrm{CSL}_0}) \ln \frac{D}{D_0} + 1} \tag{4}$$

Figure 9 shows F_{CSL} and $F_{\mathrm{CSL}}/F_{\mathrm{CSL0}}$ calculated by Equations (3) and (4), respectively, as functions of the change in the grain size (D/D_0) for different values of F_{CSL0}. The value of $K = 0.5$ was taken for the present steel. The experimental values of F_{CSL} and $F_{\mathrm{CSL}}/F_{\mathrm{CSL0}}$ are also presented in Figure 9. It is clearly seen in Figure 9 that the calculated F_{CSL} and $F_{\mathrm{CSL}}/F_{\mathrm{CSL0}}$ are in good agreement with the experimental values. It can be clearly observed that the fraction of $\Sigma 3^n$ CSL boundaries sharply rises to approximately 0.5 in the range of D/D_0 from 1 to 5, which can be considered as early stage of continuous post-dynamic recrystallization. Then, the rate of increase of F_{CSL} slows down significantly in the range of $D/D_0 > 5$. That is, the fraction of $\Sigma 3^n$ CSL boundaries tends to saturate at 0.5–0.6 in the beginning of continuous recrystallization and does not increase significantly during the following growth of recrystallized grains. Therefore, the ratio of $D/D_0 \approx 5$ can be considered as a critical condition at which the fraction of $\Sigma 3^n$ CSL boundaries approaches its apparent saturation during continuous post-dynamic recrystallization. It is interesting that Equation (3) predicts $F_{\mathrm{CSL}} \approx 1$ when D/D_0 approaches infinity. In fact, the $D/D_0 = \infty$ means that single growing grain has occupied whole sample, and therefore, only $\Sigma 3^n$ CSL boundaries are within the sample.

The fraction of $\Sigma 3^n$ CSL boundaries during annealing does not depend remarkably on the initial state, i.e. F_{CSL0}. On the other hand, the ratio of $F_{\mathrm{CSL}}/F_{\mathrm{CSL0}}$ during grain growth depends significantly on the F_{CSL0}. The experimental values of F_{CSL0} of 0.04,

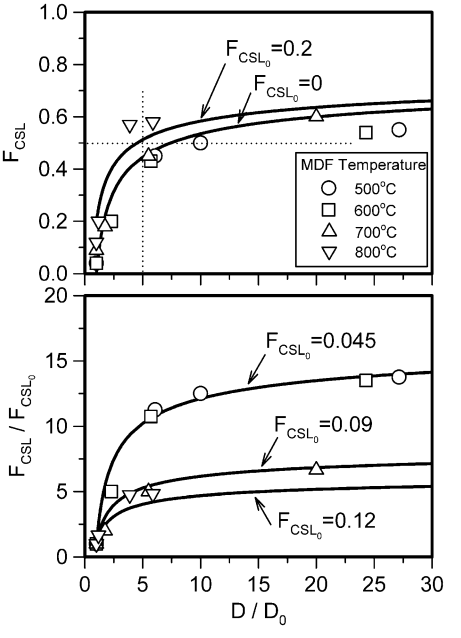

Figure 9. The relationships between the change in fraction of $\Sigma 3^n$ CSL boundaries (F_{CSL}, F_{CSL}/F_{CSL0}) and the change in grain size (D/D_0) in the S304H austenitic stainless steel subjected to MDF and annealing at different temperatures.

0.09 and 0.12 that were obtained in the samples subjected to MDF at 500–600, 700, and 800°C, respectively, were used to calculate and plot the F_{CSL}/F_{CSL0} vs. D/D_0 dependencies in Figure 9. The perfect fit of the Equation (4) to the experimental data gives proof to the above speculation of the grain boundary assembly that developed during continuous post-dynamic recrystallization.

The revealed relationship between the fraction of $\Sigma 3^n$ CSL boundaries and the change in grain size during annealing suggests a promising approach for development of ultrafine-grained metallic materials with a large fraction of special boundaries, i.e. grain boundary engineered microstructures. Such structural state can be achieved through severe plastic deformation followed by annealing at relatively low temperatures. The ultrafine-grained structures evolved by continuous dynamic recrystallization under conditions of severe plastic working are essentially stable against discontinuous static recrystallization leading to large recrystallized grains [28,29,37]. In contrast, these ultrafine-grained structures are characterized by a relatively slow grain coarsening upon subsequent annealing that is attributed to the development of continuous post-dynamic recrystallization. Since only fivefold increase in the grain size is enough for the evolution of large fraction of special boundaries, the grain boundary-engineered microstructures can be easily developed by continuous post-dynamic recrystallization, and these microstructures can be classified as being ultrafine-grained.

The presented approach can be extended to predict the fraction of special boundaries in other face centred cubic metals and alloys with low SFE subjected to various

thermo-mechanical treatments. For instance, a primary recrystallization is frequently used to obtain a large fraction of CSL boundaries [5,10,12,45–47]. The most impressive results were obtained after annealing of slightly strained samples, which were characterized by large recrystallized grains [11,46,47]. That is to say the larger recrystallized grain, the larger the CSL boundary fraction. On the other hand, the CSL boundary fraction of about 0.5 can be easily attained by an ordinary primary recrystallization leading to an average grain size of 10–20 μm, whereas further multifold increase in the recrystallized grain size provide insignificant increase in the CSL boundary fraction to 0.6–0.7 [46,47]. Therefore, the presented approach can be used to predict the fraction of special boundaries in materials subjected to conventional processing methods including cold working followed by annealing, taking appropriate values of K and D_0 (as a size of recrystallization nuclei) in Equation (3).

5. Conclusions

The characteristics of post-dynamically recrystallized microstructures in a 304-type ultrafine-grained austenitic stainless steel processed by warm MDF were studied after annealing at 800–1,000°C. The main results can be summarized as follows:

(1) The annealing behaviour of the ultrafine-grained structures, which were evolved by continuous dynamic recrystallization during large strain warm deformation, is characterized by the development of continuous post-dynamic recrystallization involving a rapid recovery and a gradual grain growth. The kinetics of continuous recrystallization that occurs in ultrafine-grained structures slows down with an increase in the temperature of the preceding deformation.
(2) The grain growth during post-dynamic recrystallization was accompanied by an increase in the fraction of $\Sigma 3^n$ CSL boundaries, which was defined by a relative change in the grain size, i.e. a ratio of the annealed grain size to that evolved by preceding warm working (D/D_0). A fivefold increase in the grain size during continuous post-dynamic recrystallization is accompanied by a rise in the fraction of $\Sigma 3^n$ CSL boundaries to 0.5. Then, the rate of increase in the fraction of $\Sigma 3^n$ CSL boundaries slowed down significantly in the range of $D/D_0 > 5$.
(3) Warm MDF to large strains followed by an annealing is a promising method for producing a bulky ultrafine-grained austenitic stainless steel with a large fraction of $\Sigma 3^n$ CSL boundaries.

Acknowledgements

The authors are grateful to the personnel of the Joint Research Centre, Belgorod State University, for their assistance with instrumental analysis.

Funding

The financial support received from the Ministry of Education and Science, Russia (project no. 14.A18.21.1844) is gratefully acknowledged.

References

[1] T. Watanabe, Res. Mech. 11 (1984) p.47.
[2] G. Gottstein, D.A. Molodov, M. Winning and L.S. Shvindlerman, Interface Sci. 9 (2001) p.297.
[3] V. Randle, Acta Mater. 52 (2004) p.4067–4081.
[4] W.G. Wang, F. Yin, H. Guo, H. Li and B. Zhou, Mater. Sci. Eng. A 491 (2008) p.199.
[5] X. Fang, W. Wang, Z. Cai, C. Qin and B. Zhou, Mater. Sci. Eng. A 527 (2010) p.1571.
[6] P. Lin, G. Palumbo, U. Erb and K.T. Aust, Scripta Metall. Mater. 33 (1995) p.1387.
[7] E.M. Lehockey, D. Limoges, G. Palumbo, J. Sklarchuk, K. Tomantschger and A. Vincze, J. Power Sources 78 (1999) p.79.
[8] D.L. Olmsted, S.M. Foiles and E.A. Holm, Acta Mater. 57 (2009) p.3694.
[9] V.Y. Gertsman and K. Tangri, Philos. Mag. A 64 (1991) p.1319.
[10] X. Fang, K. Zhang, H. Guo, W. Wang and B. Zhou, Mater. Sci. Eng. A 487 (2008) p.7.
[11] W.G. Wang, B.X. Zhou, G.S. Rohrer, H. Guo and Z.X. Cai, Mater. Sci. Eng. A 527 (2010) p.3695.
[12] X. Fang, Z. Liu, M. Tikhonova, A. Belyakov and W. Wang, J. Mater. Sci. 48 (2013) p.997.
[13] R.Z. Valiev, Nature 419 (2002) p.887.
[14] Y. Kimura, T. Inoue, F. Yin and K. Tsuzaki, Science 320 (2008) p.1057.
[15] S. Zherebtsov, E. Kudryavtsev, S. Kostjuchenko, S. Malysheva and G. Salishchev, Mater. Sci. Eng. A 536 (2012) p.190.
[16] S.V. Dobatkin, V.F. Terent'ev, W. Skrotzki, O.V. Rybalchenko, M.N. Pankova, D.V. Prosvirnin and E.V. Zolotarev, Russian Metall. (Metally) 2012 (2012) p.954.
[17] F.J. Humphreys, P.B. Prangnell, J.R. Bowen, A. Gholinia and C. Harris, Phil. Trans. R. Soc. Lond. A 357 (1999) p.1663.
[18] R.Z. Valiev, Y. Estrin, Z. Horita, T.G. Langdon, M.J. Zechetbauer and Y.T. Zhu, JOM 58 (2006) p.33.
[19] N. Tsuji, Adv. Eng. Mater. 12 (2010) p.701.
[20] Y. Estrin and A. Vinogradov, Acta Mater. 61 (2013) p.782.
[21] A. Belyakov, T. Sakai, H. Miura and K. Tsuzaki, Philos. Mag. A 81 (2001) p.2629.
[22] T. Sakai T and J.J. Jonas, in *Encyclopedia of Materials: Science and Technology*, K.H. Buschow, R.W. Cahn, M.C. Flemings, B. Ilschner, E.J. Kramer, S. Mahajan, eds., Vol. 7, Elsevier, Oxford, 2001, p. 7079.
[23] A.M. Wusatowska-Sarnek, J. Eng. Mater. Technol. 127 (2005) p.295.
[24] G.A. Salishchev, S.Y. Mironov and S.V. Zherebtsov, Rev. Adv. Mater. Sci. 11 (2006) p.152.
[25] N. Dudova, A. Belyakov, T. Sakai and R. Kaibyshev, Acta Mater. 58 (2010) p.3624.
[26] M. Tikhonova, R. Kaibyshev, X. Fang, W. Wang and A. Belyakov, Mater. Character. 70 (2012) p.14.
[27] M. Tikhonova, A. Belyakov and R. Kaibyshev, Mater. Sci. Eng. A 564 (2013) p.413.
[28] A. Belyakov, T. Sakai, H. Miura, R. Kaibyshev and K. Tsuzaki, Acta Mater. 50 (2002) p.1547.
[29] A. Belyakov, K. Tsuzaki, Y. Kimura and Y. Mishima, J. Mater. Res. 22 (2007) p.3042.
[30] T. Sakai and M. Ohashi, Mater. Sci. Technol. 6 (1990) p.1251.
[31] A. Belyakov, K. Tsuzaki, H. Miura and T. Sakai, Mater. Sci. Forum 426–432 (2003) p.1005.
[32] I. Nikulin, A. Kipelova, S. Malopheyev and R. Kaibyshev, Acta Mater. 60 (2012) p.487.
[33] P. Cizek, Mater. Sci. Forum 753 (2013) p.66.
[34] J.K. Mackenzie, Biometrika 45 (1958) p.229.
[35] J.E. Bailey and P.B. Hirsch, Proc. Roy. Soc. London A 267 (1962) p.11.
[36] F.J. Humphreys and M. Hatherly, *Recrystallization and Related Annealing Phenomena*, 2nd ed., Elsevier, Oxford, 2004.

[37] T. Sakai, A. Belyakov, R. Kaibyshev, H. Miura and J.J. Jonas, Prog. Mater. Sci. 60 (2014) p.130.
[38] S.L. Lee and N.L. Richards, Mater. Sci. Eng. A 405 (2005) p.74.
[39] J.R. Cahoon, Q. Li, N.L. Richards, Mater. Sci. Eng. A 526 (2009) p.56.
[40] Y. Jin, B. Lin, M. Bernacki, G.S. Rohrer, A.D. Rollett and N. Bozzolo, Mater. Sci. Eng. A 597 (2014) p.295.
[41] S. Mahajan, Scripta Mater. 68 (2013) p.95.
[42] C.S. Pande, M.A. Imam and B.B. Rath, Metall. Trans. A 21 (1990) p.2891.
[43] S. Mahajan, C.S. Pande, M.A. Imam and B.B. Rath, Acta Mater. 45 (1997) p.2633.
[44] C.S. Pande and M.A. Imam, Mater. Sci. Eng. A 512 (2009) p.82.
[45] M. Shimada, H. Kokawa, Z.J. Wang, Y.S. Sato and I. Karibe, Acta Mater. 50 (2002) p.2331.
[46] R. Jones and V. Randle, Mater. Sci. Eng. A 527 (2010) p.4275.
[47] B. Li and S. Tin, Mater. Sci. Eng. A 603 (2014) p.104.